X International Conference on Computational Methods for Coupled Problems in Science and Engineering
COUPLED PROBLEMS 2023
M. Papadrakakis, B. Schrefler and E. Oñate (Eds)

A MECHANOBIOLOGICAL BONE REMODELLING MODEL COUPLING BONE PHYSIOLOGY AND SYSTEMIC CALCIUM AND PHOSPHORUS HOMEOSTASIS

JAVIER MARTÍNEZ-REINA*, JOSÉ L. CALVO-GALLEGO*, FERNANDO GUTIÉRREZ-MILLÁN* AND PETER PIVONKA†

*Departmento de Ingeniería Mecánica y Fabricación
Universidad de Sevilla
Camino de los Descubrimientos s/n, 41092, Spain
e-mail: jmreina@us.es

†School of Mechanical, Medical and Process Engineering
Queensland University of Technology
Gardens Point Campus, 4000 Queensland, Australia

Key words: Bone remodelling, Cell population model, Calcium homeostasis, Hyperparathyroidism, Calcitriol, Renal deficiency, Osteoporosis

Abstract. In this work we couple a physiologically based mathematical model of integrated calcium and phosphorus homeostasis to a cell population bone remodelling model and to a pharmacokinetics (PK) - pharmacodynamics (PD) model of denosumab (Dmab), an antiresorptive drug administered to combat osteoporosis (OP). The model of Ca and P homeostasis allows to incorporate the effect of factors such as Ca dietary changes, vitamin D supplementation, concurrence of renal deficiency or hyperparathyroidism into the study of OP and its treatment.

1 INTRODUCTION

Bone remodelling (BR) models can be used to simulate the response of bone to various diseases such as OP and also to its treatment with drugs [1, 2, 3, 4, 5]. In the case of antiresorptive treatments, bone mass gain is mainly explained by mineralisation of the existing tissue, which is influenced by the amount of calcium and phosphorus available in the bone marrow. The concentrations of both ions are regulated at four levels: 1) intestinal absorption, which controls the input of ions into the serum, 2) filtration in the kidney, which regulates their excretion into the urine compartment, 3) bone resorption, that constitutes a mechanism for recovery of the mineral stored within bone matrix and 4) mineralisation of the newly formed bone tissue, when Ca and P are deposited in bone matrix. These processes are regulated by hormones secreted by the endocrine system and by diet (mainly calcium and vitamin D intake). The concurrence of osteoporosis with endocrine and dietary disorders can accelerate the disease progression and compromise the effectiveness of treatments against OP, which justifies the need for a detailed study of the coupling between all processes.

In this work, a previously developed mechanobiological model of BR [4] has been coupled with a physiological model of the regulation of Ca and P homeostasis [6]. The former includes

a model of mechanical feedback that allows to study the influence of physical activity on the treatment of OP. It also includes a model of fatigue damage accumulation in bone matrix and damage repair through bone resorption. This enables the estimation of fracture risk in osteoporotic patients with and without treatment. The coupling with the Ca and P homeostasis model has made it possible to analyse the effect of changes in the diet and the concurrence of OP with other diseases along with the efficacy of drug treatments in all these cases.

2 MATERIALS AND METHODS

2.1 Bone remodelling model

One of the main purposes of bone remodelling models is to assess the evolution of porosity, p, or alternatively the bone volume fraction f_{bm}:

$$f_{bm} = \frac{V_{bm}}{V_t} = \frac{V_t - V_p}{V_t} = 1 - p \tag{1}$$

where V_t, V_p and V_{bm} stand for the total volume of the representative volume element (RVE), the volume occupied by the pores and by the bone matrix, respectively.

Following the approach taken by Martin et al. [7], the bone remodelling process can be described as cell balance equations. The bone cell types (i.e. state variables) considered in the current model are: osteoblast precursor cells ($\mathrm{Ob_p}$), active osteoblasts ($\mathrm{Ob_a}$), osteoclast precursor cells ($\mathrm{Oc_p}$), active osteoclasts ($\mathrm{Oc_a}$) and osteocytes (Ot). The cell pools of uncommitted progenitor cells of both lineages ($\mathrm{Ob_u}$, $\mathrm{Oc_u}$) were assumed constant:

$$\frac{d\,\mathrm{Ob_p}}{dt} = D_{\mathrm{Ob_u}} \cdot \mathrm{Ob_u} \cdot \pi^{\mathrm{TGF-\beta}}_{\mathrm{act,Ob_u}} - D_{\mathrm{Ob_p}} \cdot \mathrm{Ob_p} \cdot \pi^{\mathrm{TGF-\beta}}_{\mathrm{rep,Ob_p}} + P_{\mathrm{Ob_p}} \cdot \mathrm{Ob_p} \cdot \pi^{\mathrm{Wnt}}_{\mathrm{act,Ob_p}} \tag{2}$$

$$\frac{d\,\mathrm{Ob_a}}{dt} = D_{\mathrm{Ob_p}} \cdot \mathrm{Ob_p} \cdot \pi^{\mathrm{TGF-\beta}}_{\mathrm{rep,Ob_p}} - \Delta_{\mathrm{Ob_a}} \cdot \mathrm{Ob_a} \tag{3}$$

$$\frac{d\,\mathrm{Oc_p}}{dt} = D_{\mathrm{Oc_u}} \cdot \mathrm{Oc_u} \cdot \pi^{\mathrm{RANKL}}_{\mathrm{act,Oc_u}} - D_{\mathrm{Oc_p}} \cdot \mathrm{Oc_p} \cdot \pi^{\mathrm{RANKL}}_{\mathrm{act,Oc_p}} \tag{4}$$

$$\frac{d\,\mathrm{Oc_a}}{dt} = D_{\mathrm{Oc_p}} \cdot \mathrm{Oc_p} \cdot \pi^{\mathrm{RANKL}}_{\mathrm{act,Oc_p}} - A_{\mathrm{Oc_a}} \cdot \mathrm{Oc_a} \cdot \pi^{\mathrm{TGF-\beta}}_{\mathrm{act,Oc_p}} \tag{5}$$

$$\frac{d\,\mathrm{Ot}}{dt} = \eta\, \frac{d\,f_{bm}}{dt} \tag{6}$$

where D_{X} stand for the differentiation rates of cellular stage X into the subsequent stage; $A_{\mathrm{Oc_a}}$ is the apoptosis rate of $\mathrm{Oc_a}$ and $\Delta_{\mathrm{Ob_a}}$ is the rate of clearance of active osteoblasts through apoptosis or differentiation into osteocytes. The variables $\pi^{\mathrm{TGF-\beta}}_{\mathrm{act,Ob_u}}$, $\pi^{\mathrm{TGF-\beta}}_{\mathrm{rep,Ob_p}}$ and $\pi^{\mathrm{TGF-\beta}}_{\mathrm{act,Oc_p}}$ represent activator and repressor functions related to the binding of TGF-β to its receptor. Similarly, $\pi^{\mathrm{RANKL}}_{\mathrm{act,Oc_u}}$ and $\pi^{\mathrm{RANKL}}_{\mathrm{act,Oc_p}}$ are the activator functions related to the RANK-RANKL binding. Finally, $P_{\mathrm{Ob_p}}$ is the proliferation rate of $\mathrm{Ob_p}$, a process which is mediated by the Wnt signalling pathway through the activator function π^{Wnt}_{act,Ob_p} and is described in detail in [4] along with other features of the model. A scheme of the BR model is presented in Fig. 1 (right). Eq. (6) establishes that the population of osteocytes varies proportional to the bone volume fraction f_{bm}, since the density of osteocytes within the bone matrix, η, is assumed constant as done in [7]. Finally, the activity of osteoclasts and osteoblasts determines the variation of f_{bm} through the balance between resorbed and formed tissue:

$$\frac{df_{bm}}{dt} = -k_{res} \cdot \mathrm{Oc_a} + k_{form} \cdot \mathrm{Ob_a} \tag{7}$$

where k_{res} and k_{form} are, respectively, the rates of bone resorption and osteoid formation. The RANKL-RANK-OPG signalling pathway controls the differentiation of osteoclasts through $\pi_{\mathrm{act,X}}^{\mathrm{RANKL}}$ functions:

$$\pi_{\mathrm{act,X}}^{\mathrm{RANKL}} = \frac{[\mathrm{RANKL}]}{K_{\mathrm{act,X}}^{\mathrm{RANKL}} + [\mathrm{RANKL}]} \qquad \text{with X} = \mathrm{Oc_u},\, \mathrm{Oc_p} \tag{8}$$

These are monotonically increasing functions of [RANKL], the concentration of free RANKL, which can be obtained from the competitive binding equations of the RANKL-RANK-OPG signalling pathway:

$$\begin{aligned}[\mathrm{RANKL}] = & P_{\mathrm{RANKL}} \cdot \Bigg[\tilde{D}_{\mathrm{RANKL}} + \frac{\tilde{D}_{\mathrm{OPG-RANKL}}}{K_{\mathrm{OPG-RANKL}}} \cdot [\mathrm{OPG}] \\ & + \frac{\tilde{D}_{\mathrm{RANK-RANKL}}}{K_{\mathrm{RANK-RANKL}}} \cdot [\mathrm{RANK}] + \frac{\tilde{D}_{\mathrm{Dmab-RANKL}}}{K_{\mathrm{RANKL-Dmab}}} \cdot [\mathrm{Dmab}]_{\mathrm{BC}} \Bigg]^{-1} \end{aligned} \tag{9}$$

where $\tilde{D}_X$, $\tilde{D}_{X-Y}$ and K_{X-Y} designate, respectively, the degradation rate of species X, of the compound $X-Y$ and the dissociation constant of the latter. $[\mathrm{Dmab}]_{\mathrm{BC}}$ designates the concentration of Dmab in the bone compartment (BC), i.e. bone marrow. This concentration varies over time after injection and is calculated using a PK-PD model proposed in [4]. It is clear from Eq. (9) that Dmab competes with OPG and RANK for binding to RANKL, thus hindering RANK-RANKL binding and preventing the differentiation of $\mathrm{Oc_a}$. The production of RANKL is given by:

$$P_{\mathrm{RANKL}} = P_{\mathrm{RANKL}}^{\mathrm{Ot}}(d) + P_{\mathrm{RANKL}}^{\mathrm{Ob_p}}(PTH) + P_{\mathrm{RANKL}}^{\mathrm{PMO}} \tag{10}$$

where the productions of RANKL by osteocytes and osteoblast precursors are upregulated by damage (d) and PTH, respectively, and $P_{\mathrm{RANKL}}^{\mathrm{PMO}}$ accounts for the production due to the oestrogen deficiency (OD) causing postmenopausal osteoporosis (PMO) (see [4] for details).

2.2 Damage and mineral content of bone matrix. Apparent density and stiffness

Continuum Damage Mechanics considers the accumulation of microcracks in the RVE through a damage variable $d \in [0,1]$ which is related to the microcrack density and to the degradation of stiffness, so that the current (E) and the initial or intact Young's modulus (E_0) are related by the relation $E = (1-d)\,E_0$ and $d=0$ corresponds to an undamaged state while $d=1$ corresponds to local failure. Damage can grow by fatigue and is repaired by osteoclastic resorption that dissolves the damaged tissue to be replaced later by new tissue deposited by osteoblasts. Thus, the increment of damage is obtained following [8] through the balance equation:

$$\Delta d = \underbrace{\frac{C_1}{C_2\,\gamma_t}\,(1-d)^{1-\gamma_t}\,\exp\big(-C_2\,(1-d)^{\gamma_t}\big)\,\varepsilon_{max}^{\delta_t}\,N}_{\text{Fatigue accumulation}} - \underbrace{d\,\frac{k_{res}\,\mathrm{Oc_a}}{f_{bm}}}_{\text{Repair by resorption}} \tag{11}$$

where N is the number of daily cycles of the normal activity that produces a maximum principal strain ε_{max}. C_2, δ_t and γ_t are constants and C_1 is a function of the mineral content of bone matrix. This mineral content is measured using the ash fraction, α, equal to the quotient between the mass of mineral and the dry mass, or sum of the mass of mineral and mass of

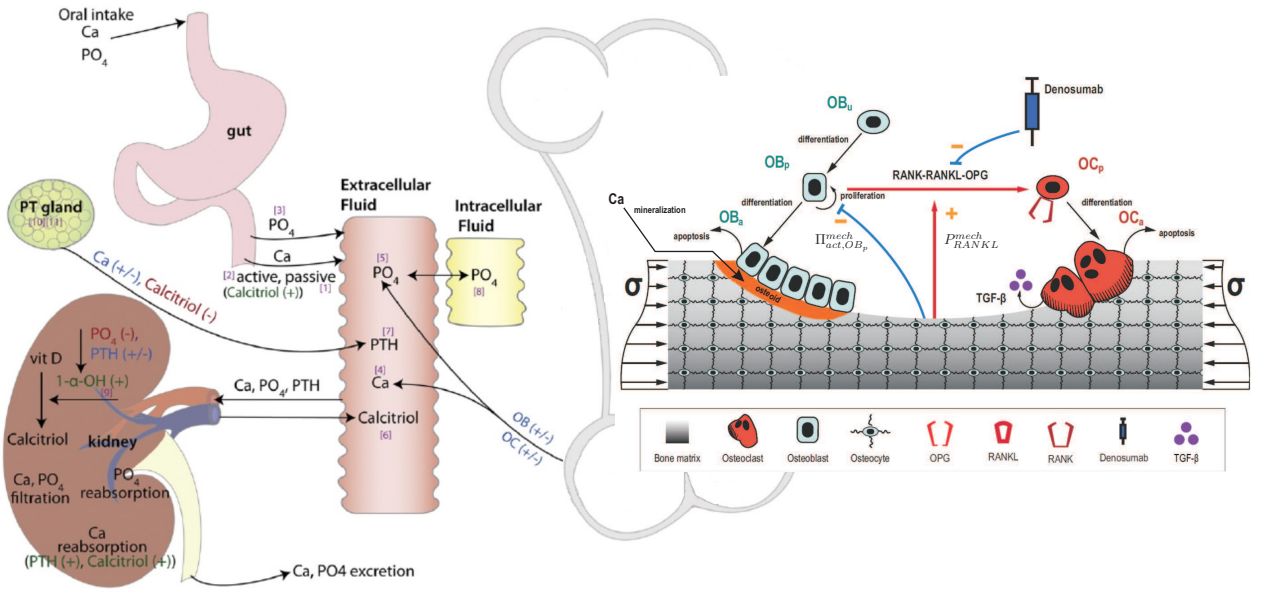

Figure 1: Schematic integration of the model of Ca and P homeostasis [6] (left) and the cell population bone remodelling model [1] (right) that replaces the bone compartment in the former model.

organic phase. The average mineral content is evaluated taking into account the mineralisation of the existing tissue, the removal of mineralised tissue by bone resorption and the formation of osteoid, the tissue laid *de novo* by osteoblasts. This initially contains only organic phase and water and begins to mineralise between 1 and 2 weeks after being deposited (see [8] for further details). The mineralisation algorithm presented in [8] has been slightly modified to account for the availability of Ca and P in bone marrow, as commented in Section 2.3.4.

Bone apparent density is given by bone volume fraction and tissue density, ρ_t, which depends on the mineral content (see for example [4]):

$$\rho = \frac{m}{V_{bm}} \frac{V_{bm}}{V_T} = \rho_t(\alpha)\ f_{bm} \tag{12}$$

Bone is assumed an isotropic material with a Poisson's ratio $\nu = 0.3$ and a Young's modulus given in MPa by the following correlations [9]:

$$E(\rho, d) = \begin{cases} 2014\,\rho^{2.5}\,(1-d) & \text{if } \rho < 1.2\ \text{g/cm}^3 \\ 1763\,\rho^{3.2}\,(1-d) & \text{if } \rho \geq 1.2\ \text{g/cm}^3 \end{cases} \tag{13}$$

A uniaxial stress state is assumed and the stiffness provided by Eq. (13) is used to calculate ε_{max}. The evolution of damage that follows Eq. (11) can be used to estimate the number of cycles needed to reach local failure ($d = 1$) for a given overload (σ) or alternatively, if the number of daily cycles is assumed constant, the number of days until failure (NDuF) and with this a fracture risk index (FRI):

$$\text{FRI}(\sigma) = \frac{100}{\text{NDuF}} \tag{14}$$

2.3 Physiologically based mathematical model of calcium and phosphorus homeostasis

The model of Peterson and Riggs [6] is depicted in Fig. 1 (left) and the list of variables considered in it is given in Table 1. The values of all the constants can be consulted in [10].

Table 1: List of variables of the adapted model of calcium and phosphorus homeostasis.

Name of variable	Description	Compartment	Initial value	Units	Comments
A_1	Ca	Gut	1.7	mmol	
A_2	Ca transporters	Gut	0.5	-	Active fraction, i.e. $A_2 \in [0,1]$
A_3	P	Gut	0.84	mmol	
A_4	Ca	Serum	32.9	mmol	
A_5	P	Serum	16.8	mmol	
A_6	Calcitriol	Serum	1340	mmol	
A_7	PTH	Serum	40.9	pmol	
A_8	P	Intracellular	3230	mmol	
A_9	Hydroxilase	Kidney	134	mmol	
A_{10}	PT pool	PT gland	0.48	-	Active fraction, i.e. $A_{10} \in [0,1]$
A_{11}	PT capacity	PT gland	1	-	Ratio capacity / normal capacity
A_{12}	Ca	Bone marrow	133	mmol	
A_{13}	Ca	Bone matrix	29706	mmol	
A_{14}	P	Bone marrow	67.5	mmol	
A_{15}	P	Bone matrix	13784	mmol	

Peterson and Riggs [6] used the following sigmoidal functions to consider the up- and downregulation effects included in their model. Thus, ${H^+}_{\mathrm{x,y}}$ and ${H^-}_{\mathrm{x,y}}$ measure, respectively, the up- and downregulation effects of the variable A_x on A_y, where the constants $\alpha_{\mathrm{x,y}}$ and $\rho_{\mathrm{x,y}}$ are the maximum and minimum values of the functions and the constants $\delta_{\mathrm{x,y}}$ and $\gamma_{\mathrm{x,y}}$ define the shape of the function. $H_{\mathrm{x,y}}$ is an upregulating function for a minimum value $\rho_{\mathrm{x,y}} = 0$.

$$H_{x,y} = \alpha_{\mathrm{x,y}} \frac{A_x^{\gamma_{\mathrm{x,y}}}}{A_x^{\gamma_{\mathrm{x,y}}} + \delta_{\mathrm{x,y}}^{\gamma_{\mathrm{x,y}}}} \tag{15}$$

$$H^+_{x,y} = \rho_{\mathrm{x,y}} + (\alpha_{\mathrm{x,y}} - \rho_{\mathrm{x,y}}) \frac{A_x^{\gamma_{\mathrm{x,y}}}}{A_x^{\gamma_{\mathrm{x,y}}} + \delta_{\mathrm{x,y}}^{\gamma_{\mathrm{x,y}}}} \tag{16}$$

$$H^-_{x,y} = \alpha_{\mathrm{x,y}} - (\alpha_{\mathrm{x,y}} - \rho_{\mathrm{x,y}}) \frac{A_x^{\gamma_{\mathrm{x,y}}}}{A_x^{\gamma_{\mathrm{x,y}}} + \delta_{\mathrm{x,y}}^{\gamma_{\mathrm{x,y}}}} \tag{17}$$

The flux of a given species from the compartment of variable A_a to the compartment of A_b is designated as $J_{\mathrm{a-b}}$ and the sigmoidal function regulating the effect of variable A_x on the flux $J_{\mathrm{a-b}}$ as $H^{\bullet}_{\mathrm{x,a-b}}$ and follows the same expressions given before. The set of differential equations that govern Ca and P homeostasis is the following:

$$\frac{dA_1}{dt} = D_1 \cdot H_{2,1} - J_{1-4} \tag{18}$$

$$\frac{dA_2}{dt} = H^+_{6,2}\,(1 - A_2) - H^-_{6,2}\,A_2 \tag{19}$$

$$\frac{dA_3}{dt} = D_3 \cdot F_3 - k_{3-5} \cdot A_3 \tag{20}$$

$$\frac{dA_4}{dt} = J_{1-4} - J_{4-u} + J_{12-4} - J_{4-12} \tag{21}$$

$$\frac{dA_5}{dt} = k_{3-5} \cdot A_3 + k_{8-5} \cdot A_8 - k_{5-8} \cdot A_5 - J_{5-u} + J_{14-5} - J_{5-14} \tag{22}$$

$$\frac{dA_6}{dt} = k_{25-OHD} \cdot A_9 - k_{6D} \cdot A_6 \tag{23}$$

$$\frac{dA_7}{dt} = H^-_{4,7} \cdot \frac{A_{10}}{0.5}\,A_{11} - k_{7D} \cdot A_7 \tag{24}$$

$$\frac{dA_8}{dt} = k_{5-8} \cdot A_5 - k_{8-5} \cdot A_8 \tag{25}$$

$$\frac{dA_9}{dt} = k_{9S} \cdot H_{7,9} \cdot H^-_{5,9} - k_{9D} \cdot A_9 \tag{26}$$

$$\frac{dA_{10}}{dt} = (1 - A_{10}) \cdot k_{10} \cdot (0.85 \cdot T^-_{6,4} + 0.15) - A_{10} \cdot k_{10} \cdot (0.85 \cdot T^+_{6,4} + 0.15) \tag{27}$$

$$\frac{d\mathrm{A}_{11}}{dt} = k_{11S} \cdot H^{-}_{6,11} - k_{11D} \cdot \mathrm{A}_{11} + k_{PTH} \tag{28}$$

$$\frac{d\mathrm{A}_{12}}{dt} = J_{4-12} - J_{12-4} + J_{13-12} - J_{12-13} \tag{29}$$

$$\frac{d\mathrm{A}_{13}}{dt} = J_{12-13} - J_{13-12} \tag{30}$$

$$\frac{d\mathrm{A}_{14}}{dt} = J_{5-14} - J_{14-5} + J_{15-14} - J_{14-15} \tag{31}$$

$$\frac{d\mathrm{A}_{15}}{dt} = J_{14-15} - J_{15-14} \tag{32}$$

where k_{x-y}, k_{xS} and k_{xD} are constants controlling, respectively, the flux from x to y and the storage and degradation of x. The rest of constants and functions are described next.

2.3.1 Ca and P absorption

The variation of Ca and P in the gut are given by Eqs. (18) and (20) respectively, where D_1 and D_3 are the corresponding dietary intakes. Ca absorption in the gut is regulated via $H_{2,1}$ by Ca transporters, A_2 (see Eq. (18)), that also control the absorption to the blood serum through:

$$J_{1-4} = \underbrace{k_{1-4} \cdot \mathrm{A}_1}_{\text{Passive absorption}} + \underbrace{H_{1,1-4} \cdot \frac{\mathrm{A}_2}{0.5} \cdot \frac{\mathrm{A}_1}{\delta_{2,1}+\mathrm{A}_1}}_{\text{Active absorption}} \tag{33}$$

The activation/deactivation of Ca transporters is regulated by calcitriol through Eq. (19). The absorption of P was assumed in [6] to be unregulated. The variation of Ca in the serum is obtained through the balance between the fluxes of the different compartments that exchange Ca with the central compartment (see Eq. (21)). A_{12} and A_{14} designated in Peterson and Riggs' model the amount of Ca stored in the bone compartment, respectively in the so-called immediately exchangeable and non-immediately exchangeable compartments. We have assumed here that A_{12} and A_{14} comprise the Ca contained in bone marrow and bone matrix, respectively. Analogously, A_{13} and A_{15} comprise the P ions contained in the bone marrow and the bone matrix, respectively. The volume of distribution of the compartments is different and are taken into account to define the fluxes as proportional to the concentrations, in contrast to [6]. For instance, the flux of Ca from bone marrow to serum is proportional to the amount A_{12} divided by the volume of bone marrow, V_p, which varies as a result of bone remodelling and the inverse flux includes a saturation factor, with a reference concentration $\mathrm{A}_{12}^{\max}/V_p^*$ over which no calcium can enter the bone marrow compartment:

$$J_{12-4} = k_{12-4} \, \frac{\mathrm{A}_{12} \, V_p^*}{V_p} \tag{34}$$

$$J_{4-12} = k_{4-12} \, \mathrm{A}_4 \left(1 - \frac{\mathrm{A}_{12}/V_p}{\mathrm{A}_{12}^{\max}/V_p^*}\right) \tag{35}$$

where V_p^* is a reference volume of pores introduced to preserve the units of constant k_{12-4} as in [6]. The variation of P in the serum (Eq. (22)) is obtained similarly to Eq. (21).

Peterson and Riggs modelled the exchange fluxes of P between the serum and the bone compartment as proportional to the corresponding fluxes of Ca, with the stoichiometric relation between P and Ca in hydroxyapatite ($r_{P/Ca} = 0.464$) being the proportionality constant. This is equivalent to consider that the species being exchanged is hydroxyapatite, but this should

only apply for the exchange between bone marrow and bone matrix. Therefore, the exchange of P between serum and bone marrow is modelled here with equations analogous to (34) and (35):

$$J_{14-5} = k_{14-5}\,\frac{\mathrm{A}_{14}\,V_p^*}{V_p} \tag{36}$$

$$J_{5-14} = k_{5-14}\,\mathrm{A}_5\,\left(1 - \frac{\mathrm{A}_{14}/V_p}{\mathrm{A}_{14}^{\max}/V_p^*}\right) \tag{37}$$

2.3.2 Ca and P excretion

The flux of Ca to urine (J_{4-u}) is downregulated by calcitriol, through $\mathrm{H}_{6,4}$ and is proportional to the concentration of Ca in serum, while the amount reabsorbed is PTH-dependent, through $\mathrm{H}_{7,4-\mathrm{u}}$. The flux of P to urine (J_{5-u}) considers a threshold (φ_{5-u}) as in [6]:

$$J_{4-u} = k_{4-u}\,(2 - H_{6,4})\,\left(0.3 \cdot GFR \cdot \frac{\mathrm{A}_4}{V_{serum}} - H_{7,4-u}\right) \tag{38}$$

$$J_{5-u} = k_{5-u} \cdot GFR \cdot \max\left(\mathrm{A}_5 - \varphi_{5-\mathrm{u}}, 0\right) \tag{39}$$

where GFR is the glomerular filtration rate that can be impaired in the case of renal deficiency.

2.3.3 Calcitriol, 1-α-hydroxylase and PTH

The variation of serum calcitriol is governed by Eq. (23), where the first term considers the hydroxylase (A_9) mediated transformation of calcidiol (constant k_{25-OHD}) into calcitriol taking place in the kidneys. The variation of serum PTH is given by Eq. (24), where the production of PTH is downregulated by serum Ca through $H_{4,7}^-$ and controlled by the size of the PT glands A_{11} and the proportion of active PT cells A_{10}. The variation of 1-α-hydroxylase in the kidneys is given by Eq. (26), upregulated by serum PTH ($H_{7,9}$) and downregulated by serum P ($H_{5,9}^-$). The growth of the PT glands is downregulated by calcitriol through $H_{6,11}^-$ in Eq. (28) and the activation of the PT cells (Eq. (27)) is downregulated by serum Ca and calcitriol through:

$$T_{6,4}^{\pm} = 1 \pm \tanh\left(b_{T_{6,4}}\left(\frac{\mathrm{A}_6}{V_{serum}} - \delta_{T_{6,4}} \cdot \left(\frac{\mathrm{A}_{40}}{\mathrm{A}_4}\right)^{\gamma_{4,10}}\right)\right) \tag{40}$$

2.3.4 Exchange of Ca and P between bone marrow and bone matrix

In Eqs. (29)-(32) the fluxes of P and Ca from bone marrow to bone matrix correspond to the formation of hydroxyapatite crystals and the inverse fluxes to the dissolution of those crystals through osteoclastic resorption. Therefore, they are related by the stoichiometric ratio $r_{P/Ca}$. In the case of mineralisation the fluxes J_{12-13} and J_{14-15} are further constrained by the limiting species, either P or Ca:

$$J_{12-13} = \begin{cases} k_{12-13}\,\mathrm{A}_{12}\,\frac{V_p^*}{V_p}\,\left(1 - \frac{\mathrm{A}_{13}}{\mathrm{A}_{13}^{\max}}\right) & \text{if } \mathrm{A}_{12} \cdot r_{P/Ca} \le \mathrm{A}_{14} \\ \frac{J_{14-15}}{r_{P/Ca}} & \text{if } \mathrm{A}_{12} \cdot r_{P/Ca} > \mathrm{A}_{14} \end{cases} \tag{41}$$

$$J_{14-15} = \begin{cases} J_{12-13} \cdot r_{P/Ca} & \text{if } \mathrm{A}_{12} \cdot r_{P/Ca} \le \mathrm{A}_{14} \\ k_{14-15}\,\mathrm{A}_{14}\,\frac{V_p^*}{V_p}\,\left(1 - \frac{\mathrm{A}_{15}}{\mathrm{A}_{15}^{\max}}\right) & \text{if } \mathrm{A}_{12} \cdot r_{P/Ca} > \mathrm{A}_{14} \end{cases} \tag{42}$$

Table 2: Description of the modifications introduced in the model to analyse the different scenarios simulated.

Case	Description	Start time
Extra calcium intake	D_1 in Eq. (18) increased by 10%	t=0
Supplement of vitamin D	k_{25-OHD} in Eq. (23) increased by 10%	t=0
Exercise	Homeostatic load increased by 25%	t=10 years
Dmab treatment	4 injections of 60 mg every 6 months	t=10 years
Oestrogen deficiency (PMO)	$P^{\text{PMO}}_{\text{RANKL}}$ in Eq. (10) increases from 0 to $P^{\text{PMO}}_{\text{RANKL,max}}$ as in [3] $P^{\text{PMO}}_{\text{RANKL}}(t) = P^{\text{PMO}}_{\text{RANKL,max}} \frac{t}{t+\delta_{PMO}}$ with $P^{\text{PMO}}_{\text{RANKL,max}} = 10$ pM/day and $\delta_{PMO} = 1$ year	t=0
Renal deficiency	GFR in Eqs. (38),(39) decreases for 300 days from GFR_0 to GFR_{min} $GFR(t) = GFR_0 - (GFR_0 - GFR_{min}) \left[2\left(\frac{t}{300}\right) - \left(\frac{t}{300}\right)^2\right]$ with $GFR_0 = 6$ l/h, $GFR_{min} = 1$ l/h and t in days, as in [6]	t=0
Hyperparathyroidism	k_{PTH} in Eq. (28) increases for 300 days from 0 to $k_{PTH,max}$ $k_{PTH}(t) = k_{PTH,max} \left[2\left(\frac{t}{300}\right) - \left(\frac{t}{300}\right)^2\right]$ with $k_{PTH,max} = 0.03$ h^{-1} and t in days, analogously to GFR	t=0

For example, the first condition in both equations applies if there is enough P in the bone marrow to form hydroxyapatite crystals during the mineralisation process, i.e. the limiting species is Ca. In such case, the flux of Ca (J_{12-13}) is limited by the saturation factor in parentheses and the flux of P (J_{14-15}) is limited by the stoichiometric ratio. The second condition applies if the limiting species is P and the restrictions are reversed. The fluxes of P and Ca from bone matrix to bone marrow are governed by bone resorption:

$$J_{13-12} = \frac{\text{A}_{13} \cdot k_{res} \cdot \text{Oc}_\text{a}}{f_{bm}} \tag{43}$$

$$J_{15-14} = \frac{\text{A}_{15} \cdot k_{res} \cdot \text{Oc}_\text{a}}{f_{bm}} \tag{44}$$

The mineralisation algorithm used in previous models [1, 2, 3, 4] was simply described by the flux of Ca from bone marrow to bone matrix at a constant rate, i.e. $J_{12,13} = k_{12-13}\left(1 - \frac{\text{A}_{13}}{\text{A}_{13}^{\max}}\right)$. The algorithm proposed here considers the availability of Ca and P in bone marrow as limiting factors that control the mineralisation rate.

3 RESULTS

We used the coupled model of BR and Ca and P homeostasis to analyse the behaviour of a RVE of trabecular bone with initial $f_{bm,0} = 30\%$ subjected to the homeostatic load in different scenarios: OD causing PMO, renal deficiency, hyperparathyroidism (HPT), the combination of OD with the latter two disorders and the treatment of PMO with Dmab. In the case of treatment, we also analysed the influence of an extra dietary calcium intake, a supplement of vitamin D and exercise modelled by a moderate increase of the applied load, all of them coinciding with the beginning of the treatment. The details of each modification are listed in Table 2.

Fig. 2 shows several results obtained in the simulation of the three diseases. The evolution of all variables are normalised by dividing by the initial values. In the case of renal disease, it can be seen in Fig. 2A that serum P rises steadily as a consequence of renal filtration impairment (Eq. (39)). This causes a significant decrease in hydroxylase production (through $H^-_{5,9}$ in Eq. (26)) and consequently a decrease in calcitriol production (see Fig. 2A (dashed line) and recall Eq. (23)), finally leading to a 7-fold increase in PTH levels (see Fig. 2B) mediated by the

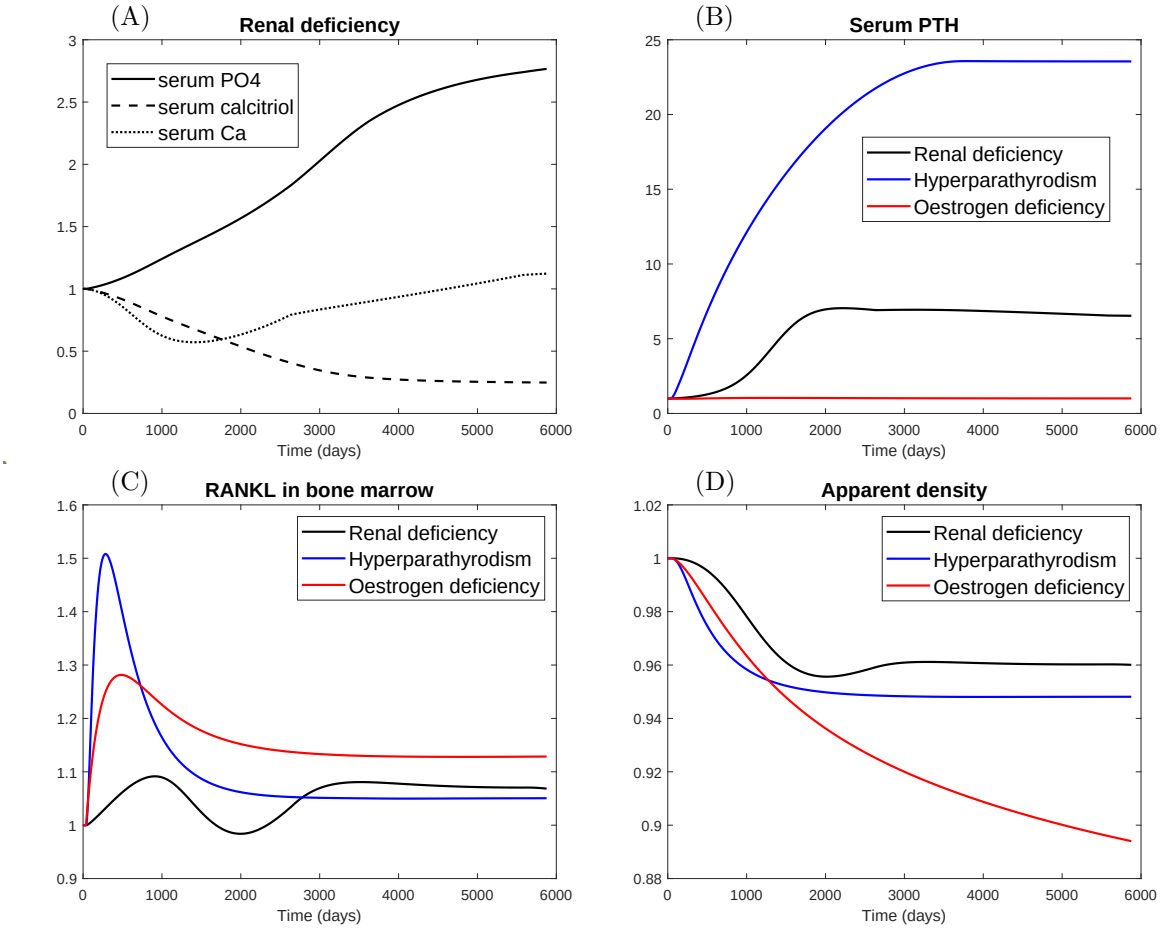

Figure 2: (A) Evolution of serum P, Ca and calcitriol in the case of renal deficiency. Evolution of serum PTH (B), RANKL in bone marrow (C), and apparent density (D) for the three diseases. In all cases, the evolution shown is relative to the initial value.

growth of PT glands (Eq. (28)). PTH upregulates the production of RANKL by $\mathrm{Ob_p}$, so that RANKL is temporarily increased until the $\mathrm{Ob_p}$ pool decreases, thus self-regulating RANKL production. While the RANKL levels are over the homeostatic value the enhanced osteoclastic activity reduces bone density up to 4% in the long term.

HPT is modelled here by an increasing growth of the PT glands (k_{PTH}) which then produce more PTH and raise its serum level very significantly (see Fig. 2B). This produces a very pronounced RANKL increase which, although attenuated in the long term as before, causes bone density to fall more steeply than in the case of renal deficiency, by more than 5%.

The OD ocurring after menopause has been reported to produce an enhanced RANKL expression by stromal cells and lymphocytes [11] which was modelled here by a sigmoidal increase or RANKL production $P^{\mathrm{PMO}}_{\mathrm{RANKL}}$. This raises RANKL levels more steadily than in the previous cases (see Fig. 2C) and produces a greater drop in bone density that in fact does not stabilize over time as in the other two diseases.

Fig. 3A shows the evolution of normalised apparent density in the case of PMO treated with Dmab and other complementary therapeutic actions starting at different stages: extra Ca intake and supplement of vitamin D begin with the onset of menopause, but exercise begins with the Dmab treatment, 10 years after menopause. Dmab injections are discontinued after

2 years, but all other therapeutic actions are maintained over time. It can be observed that Dmab increases density by approximately 4% in 2 years and that the extra Ca intake has no effect on bone gain. This is because only a small fraction of Ca is absorbed; specifically 0.5% of the 10% increase in Ca intake reaches the bone matrix. Vitamin D supplementation is more effective as it is able to increase serum calcitriol and Ca levels and this enhances Ca deposition into bone matrix through mineralisation, which increases tissue density. In addition, the rise of Ca and calcitriol serum levels reduce serum PTH (through $T^{-}_{6,4}$ and $T^{+}_{6,4}$ in Eq. (27)) so decreasing osteoclastic activity and thus slowing down the bone loss inherent to PMO. In all the above cases, a sharp drop in bone density is observed when the Dmab treatment is discontinued, except for the case of exercise when the mechanical stimulus is able to maintain bone density over time. Besides, the efficacy of the treatment is significantly enhanced with mechanical stimulus.

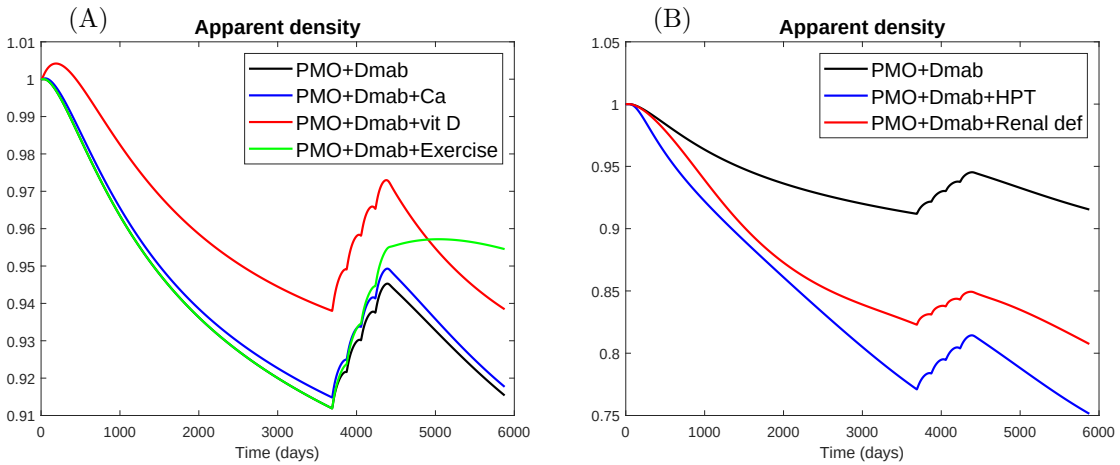

Figure 3: Evolution of apparent density relative to the initial value: (A) in the case of PMO treated with Dmab after 10 years since menopause and other complementary therapeutic actions (starting as indicated in table 2), (B) in the case of PMO concurring with other disorders from the beginning of the simulations.

Fig. 3B compares the evolution of normalised apparent density in the case of PMO alone and concurring with HPT or renal deficiency. It must be noted first that the concurrence of OD with other disorders can jeopardize bone integrity very notably, especially in the concurrence with HPT, when RANKL increases very significantly due to OD and the abnormal production of PTH. The efficacy of the treatment with Dmab when PMO and renal deficiency concur is hampered by the fact that the latter lowers serum calcitriol levels (recall Fig. 2A) and this impairs the mineralization of bone matrix, which is mainly responsible for the bone mass gain in antiresorptive treatments.

Fig. 4 shows the FRI for different scenarios and overload stresses, measured by the factor that multiplies the homeostatic stress. It can be seen in Fig. 4A that PMO increases the fracture risk for certain overload magnitudes: no fracture risk is predicted for a x4 overload (black line), but a FRI=50 is predicted for a x4.5 overload (red line). Antiresorptive treatment momentarily reduces fracture risk, which increases again upon discontinuation of the treatment, except if the applied load is moderately increased with an exercise program (blue line). The concurrence of OD with other disorders increases the fracture risk even for moderate overloads (Fig. 4B), especially in the case of HPT.

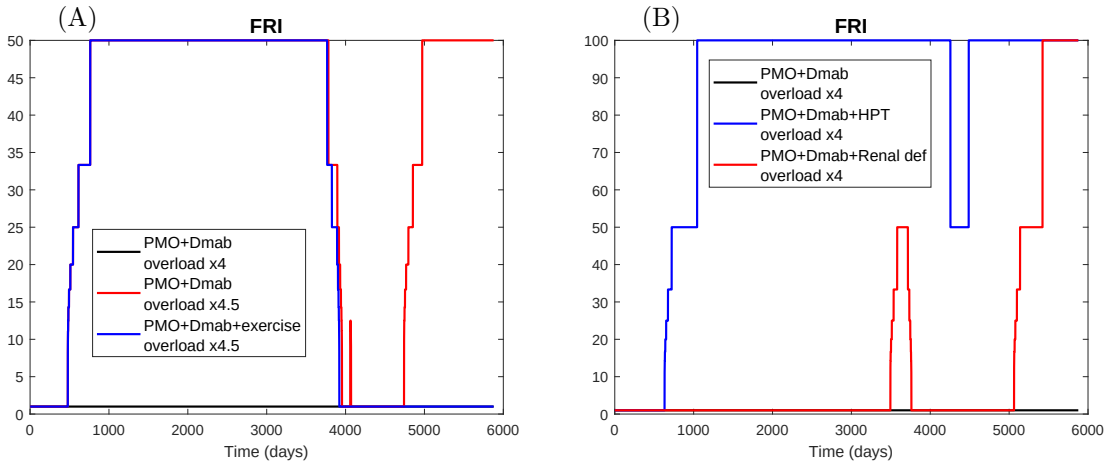

Figure 4: Risk of fracture measured with FRI for different overload magnitudes and in different scenarios.

4 CONCLUSIONS

A cell population bone remodelling model coupled with a physiologically based mathematical model of integrated calcium and phosphorus homeostasis has been used in this work to simulate different scenarios combining metabolic and endocrine disorders that can affect bone integrity. A PK-PD model of Dmab was also integrated in the coupled model to analyse the response of bone to this antiresorptive treatment.

Dmab has been shown to be effective in fighting osteoporosis by both increasing bone density and reducing the risk of fracture. Other therapeutic actions were analysed in combination with Dmab and it was found that an increase in calcium intake does not have a significant effect as does a vitamin D supplement that helps fix the mineral in bone matrix. Even more significant is the effect of physical exercise which would help to maintain bone integrity even after discontinuation of the Dmab treatment.

The concurrence of OD following menopause with other conditions such as renal deficiency or HPT is of particular concern because it accentuates bone loss and increases the fracture risk.

The coupling of these models opens the way for the patient-specific analysis of bone integrity, as well as for the design of specific treatments based on the metabolic and endocrine characteristics of the patient, treatments that may include other therapeutic actions in addition to drug treatments.

REFERENCES

[1] Martínez-Reina, J. and Pivonka, P. Effects of long-term treatment of denosumab on bone mineral density: insights from an in-silico model of bone mineralization. *Bone* (2019) **125**:87–95.

[2] Martínez-Reina, J. and Calvo-Gallego, J.L. and Pivonka, P. Are drug holidays a safe option in treatment of osteoporosis?–Insights from an in silico mechanistic PK–PD model of denosumab treatment of postmenopausal osteoporosis. *J. Mech. Behav. Biomed. Mater.* (2021) **113**: e104140.

[3] Martínez-Reina, J. and Calvo-Gallego, J.L. and Pivonka, P. Combined effects of exercise and denosumab treatment on local failure in post-menopausal osteoporosis– Insights from bone remodelling simulations accounting for mineralisation and damage. *Front. Bioeng. Biotechnol.* (2021) **9**:635056.

[4] Martínez-Reina, J. and Calvo-Gallego, J.L. and Martin, M. and Pivonka, P. Assessment of strategies for safe drug discontinuation and transition of denosumab treatment in PMO – Insights from a mechanistic PK/PD model of bone turnover. *Front. Bioeng. Biotechnol.* (2022) **10**:886579.

[5] Calvo-Gallego, J.L. and Pivonka, P. and Ruiz-Lozano, R. and Martínez-Reina, J. Mechanistic PK-PD model of alendronate treatment of postmenopausal osteoporosis predicts bone site-specific response. *Front. Bioeng. Biotechnol.* (2022) **10**:940620.

[6] Peterson, M.C. and Riggs, M.M. A physiologically based mathematical model of integrated calcium homeostasis and bone remodeling. *Bone* (2010) **46**:49–63.

[7] Martin, M. and Sansalone, V. and Cooper, D.M.L. and Forwood, M.R. and Pivonka, P. Mechanobiological osteocyte feedback drives mechanostat regulation of bone in a multiscale computational model. *Biomech. Model. Mechan.* (2019) **18**:1475-1496.

[8] Martínez-Reina, J. and García-Aznar, J.M. and Domínguez, J. and Doblaré, M. On the role of bone damage in calcium homeostasis. *J. Theor. Biol.* (2008) **254**:704–712.

[9] Jacobs, C.R. *Numerical Simulation of Bone Adaptation to Mechanical Loading*. PhD Thesis. Stanford University (1994).

[10] Gutiérrez-Millán, F. *Determinación del estímulo mecánico más apropiado para modelos de remodelación ósea. Aplicación a un modelo basado en poblaciones celulares*. MSc Thesis. Universidad de Sevilla (2022).

[11] Eghbali-Fatourechi, G. and Khosla, S. and Sanyal, A. and Boyle, W. J. and Lacey, D. L. and Riggs, B. L. Role of RANK ligand in mediating increased bone resorption in early postmenopausal women. *J. Clin. Invest.* (2003) **111**: 1221-1230.